

**MICROSTRUCTURAL EXAMINATION OF V-4Cr-4Ti PRESSURIZED TUBES - D. S. Gelles, M. L. Hamilton, and R. J. Kurtz (Pacific Northwest National Laboratory)\***

**OBJECTIVE**

The objective of this effort is to provide understanding of the processes controlling thermal creep in vanadium alloys in order to provide comparison with response under irradiation.

**SUMMARY**

Failed thermal creep pressurized tubes of V-4Cr-4Ti tested at 700 and 800°C have been examined using optical microscopy, scanning electron microscopy and transmission electron microscopy in order to understand failure and creep mechanisms. Results show extensive thinning was controlled by dislocation climb. Dislocation cell structure was not well developed, TiO<sub>2</sub> particles developed complex dislocation tangles and evidence for development of fine precipitation during creep was found.

**PROGRESS AND STATUS**

Introduction

Biaxial thermal creep response for V-4Cr-4Ti at 700 and 800°C was recently reported.<sup>1</sup> The present effort describes examination of specimens that failed using optical microscopy (OM), scanning electron microscopy (SEM) and transmission electron microscopy (TEM) techniques. The OM and SEM examinations were intended to locate the failure sites and to begin evaluating the failure mechanism. The work was extended to include microstructural examination by TEM in order to verify the controlling deformation mechanism. Creep tests at lower temperatures had shown high values for the stress dependence of secondary creep whereas grain boundary sliding could apply for the test conditions used.

Experimental Procedure

Specimens that failed during thermal creep testing of pressurized tubes are listed in Table 1.

Specimens AR15, AR17, AR18 and AR19 were examined by OM, and specimens AR18 and AR19 were examined by SEM using standard techniques. Pieces remaining after sectioning for OM and SEM were prepared for TEM by cutting 3 mm curved sections from tubes AR15, AR17 and AR19 using an ultrasonic drill, grinding the disks flat and then thinning the disks using standard electropolishing procedures in a Struers twin jet polisher. Microscopy was performed on a JEM 1200 EX using standard procedures.<sup>3</sup>

---

\* Pacific Northwest National Laboratory (PNNL) is operated by the U.S. Department of Energy by Battelle Memorial Institute under contract DE-AC06-76RLO-1830.

Table 1. Test conditions for failed pressurized tube specimens of V-4Cr-4Ti (heat 832665<sup>2</sup>).

Specimen ID	Temp. (°C)	Effective Stress (MPa)	Time to failure (hrs)	Effective mid-wall strain (%)
AR15	700	159	2804	13.0
AR17	800	93	864	13.6
AR18	800	118	578	24.1
AR19	800	137	242	14.7

## Results

### Macroscopic features

Photographs of tubes AR18 and AR19 using OM are shown in Figures 1a, and b, and c, and d, respectively. The tubes have been oriented to show the likely failure sites in the center of the tube in a) and c) and at the top of the tube in b) and d). Tubes are 27.4 mm in length. In both cases failure appears to be due to formation of a longitudinal crack.

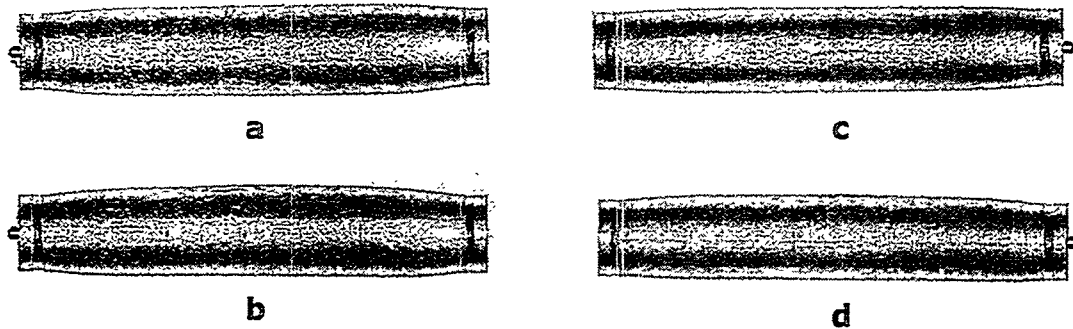


Figure 1. Failed pressurized tubes AR18 in a) and b) and AR19 in c) and d) shown with the likely failure site face-on at the top and rotated towards the top at the bottom.

The tubes were then sectioned in order to examine the failure sites from the inside of the tube. Photographs of the inner surfaces of the same specimens are provided in Figure 2, further illustrating the longitudinal failure.

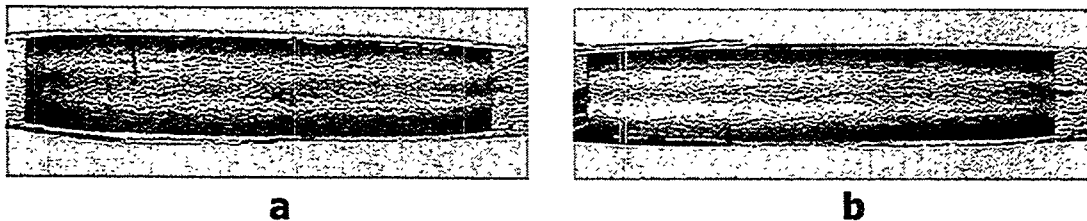


Figure 2. Failed pressurized tubes AR18 and AR19 showing the inner wall in the vicinity of the likely failure site for AR18 in a) and for AR19 in b).

SEM examination failed to conclusively identify the failure sites. The inner surfaces of specimens AR18 and AR19 were examined, and selected images are provided in Figures 3 and 4 that correspond to the photographs in Figure 2. From the low magnification examples in Figures 3 and 4, a number of fine longitudinal cracks can be identified. In each figure sequence, an area within the low magnification image has been enlarged in order to show surface features in greater detail. However, it cannot be demonstrated that these are through-thickness cracks.

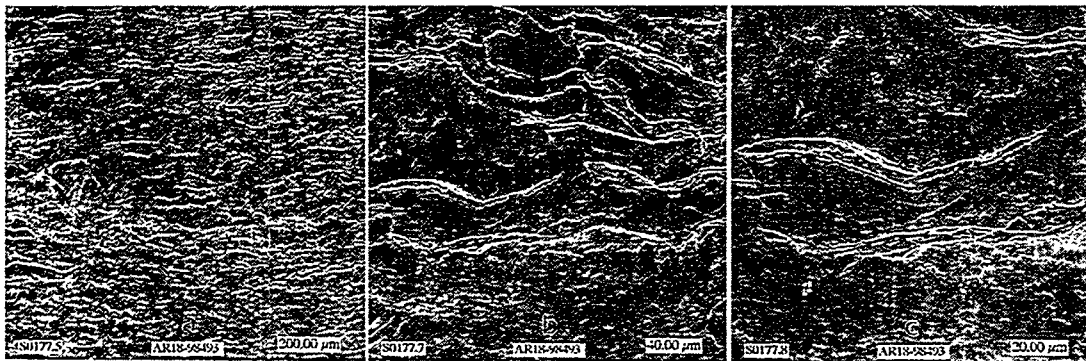


Figure 3. Surface features found on specimen AR18 at the failure location

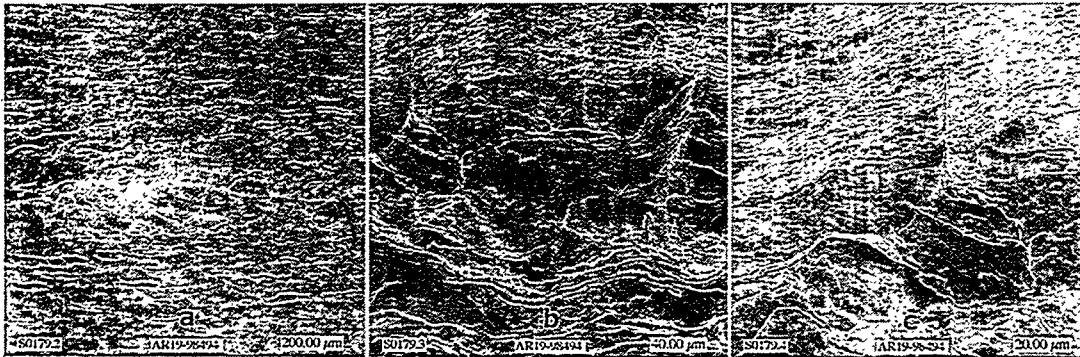


Figure 4. Surface features found on specimen AR19 at the failure location.

Metallographic sections were then prepared in order to locate through-thickness cracks. Examples are provided in Figure 5 showing regions in specimens AR15, AR17 and AR19 that contain areas that have been reduced in wall thickness between 60 and 75%. Figure 5 also includes transverse and longitudinal examples of unthinned sections of specimen AR17. From Figure 5, examples of grain elongation can be identified in each of the thinned sections, indicating that strain within grains reached high levels in comparison to grains in unthinned regions. Figure 5e) illustrates the bimodal distribution in grain size present in the tubing, i.e., the existence of a group of large grains interspersed with smaller grains.

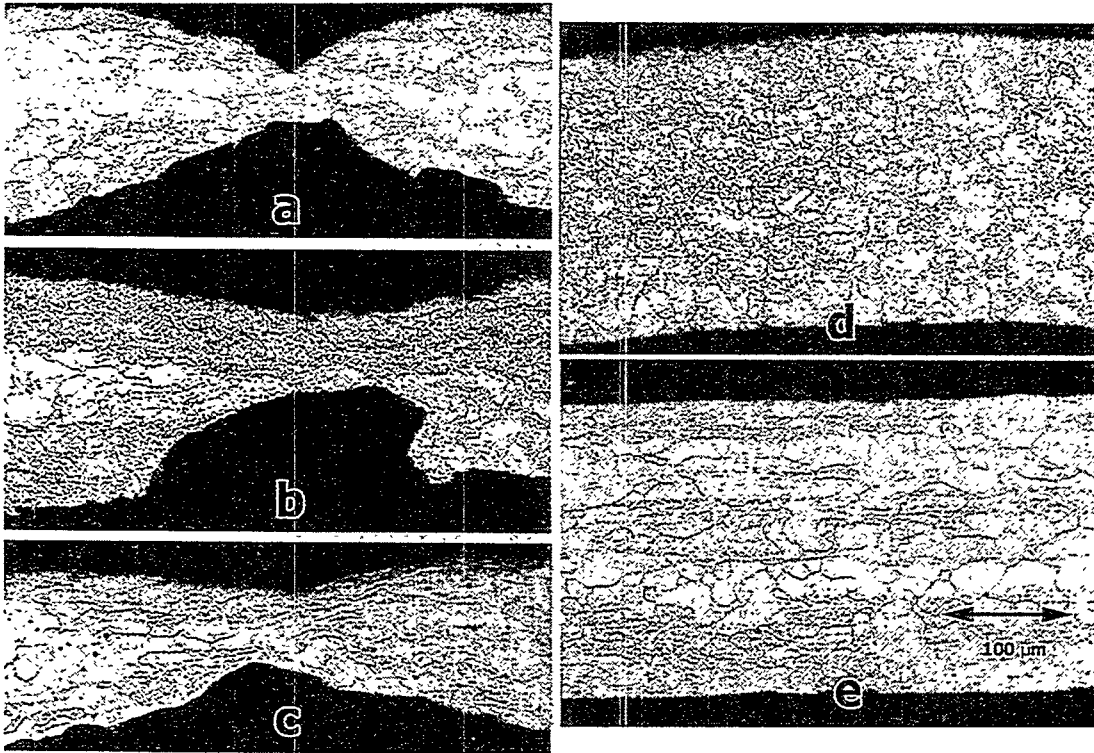


Figure 5. Optical metallographic examples of thinned sections of specimens AR15, AR17 and AR19 with unthinned transverse and longitudinal sections of specimen AR17 provided for comparison.

### Microstructure

Specimens for TEM were successfully prepared from specimens AR15, AR17 and AR19 but thin area was limited. All microstructures were found to contain a moderate density of dislocations non-uniformly distributed. However, evidence for clearly defined cell walls and therefore a cell diameter characteristic of dislocation-controlled thermal creep behavior were not found. Instead the structure contained areas with higher or lower dislocation density, depending on location. However, in the vicinity of larger  $\text{TiO}_2$  precipitate particles (~200 nm in diameter), the dislocation density was significantly higher, indicating that such particles were probably obstacles to dislocation evolution.

Examples of the microstructures found are given first for specimens tested at 800°C and then for the specimen tested at 700°C. Figure 6 shows low magnification examples of specimen AR17, tested at 800°C. Figures 6 a) and c) provide examples of grain boundary nodes indicating that most grain boundaries are straight and precipitate free, but some are heavily decorated with precipitation, presumably formed on cooling during heat treatment.<sup>4</sup> Figures 6 b) and c) indicate that the dislocation structure consists of a moderate dislocation density, but 200 nm diameter precipitate particles may be decorated at higher density. Also, figure 6 b) shows evidence of a poorly defined cell structure towards the center of the micrograph.

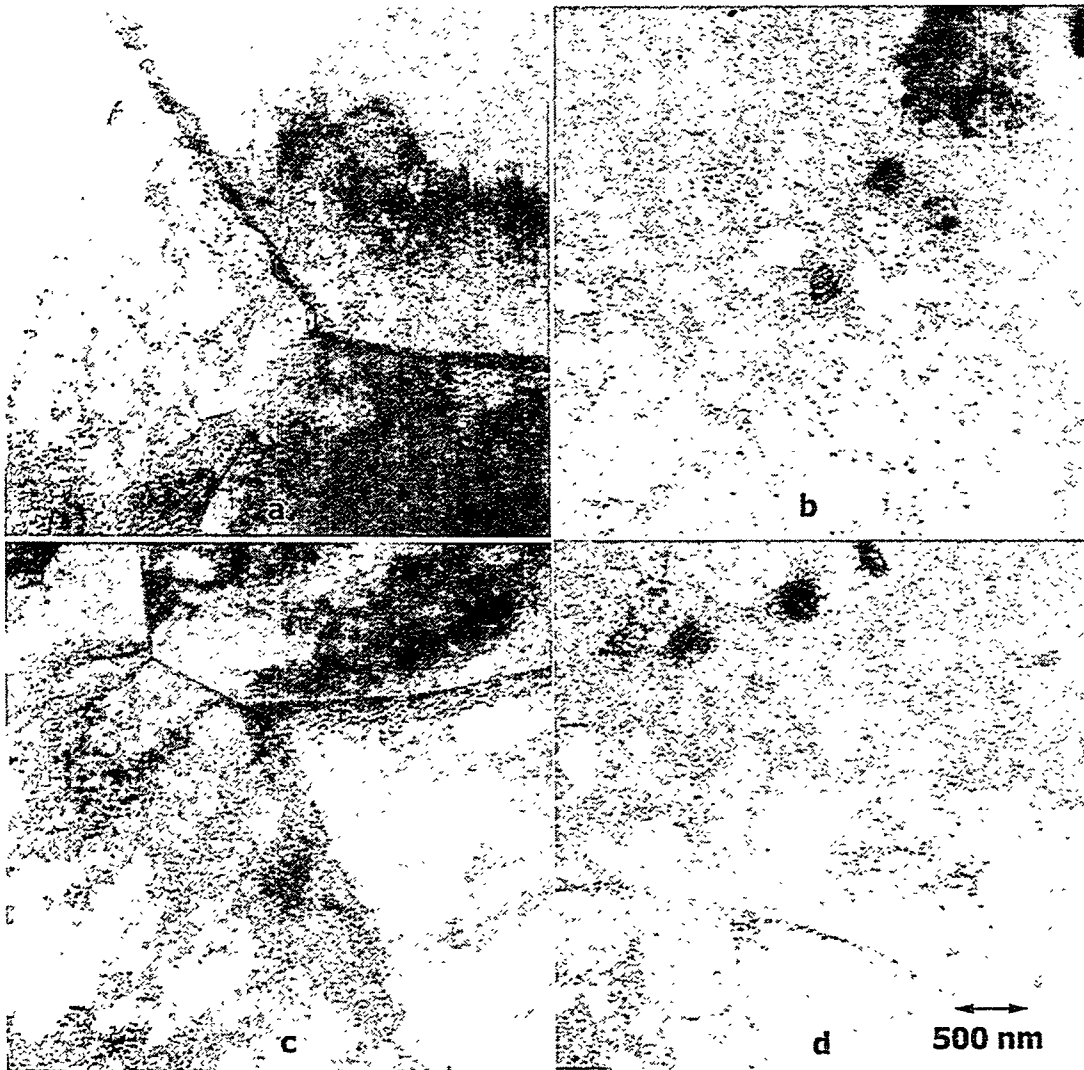


Figure 6. Low magnification examples of the microstructure of specimen AR17.

Figures 7 and 8 show the dislocation structure in greater detail for specimens AR17 and AR19, respectively. In each case, the structure is shown as a series of bright field stereo pairs, involving extensive tilting. Figures a) and b) give  $\langle 110 \rangle$  images taken near (001), Figures e) and f) give  $\langle 01\bar{1} \rangle$  in the latter do you mean bar 1? images taken near (011) and Figures c) and d) give  $\langle 002 \rangle$  images taken between (001) and (011). Assuming that dislocations in vanadium alloys are of type  $a/2 \langle 111 \rangle$ , then  $\langle 002 \rangle$  images should show all dislocations present in equal contrast, whereas  $\langle 110 \rangle$  and  $\langle 01\bar{1} \rangle$  images will only show two of the four sets, one of which will be seen in both sets of images. By process of elimination, it should therefore be possible to identify the Burgers vectors for all dislocations present.<sup>3</sup> From these figures, several observations can be made. The dislocation structure is non-uniformly distributed, with highest density near large  $\text{TiO}_2$  particles, but with formation of poorly defined cell walls, and containing lowest densities between these cell walls. However, many small dark features can be identified, believed to be precipitation of  $\text{Ti}(\text{O,C,N})$  type that formed during thermal creep exposure.

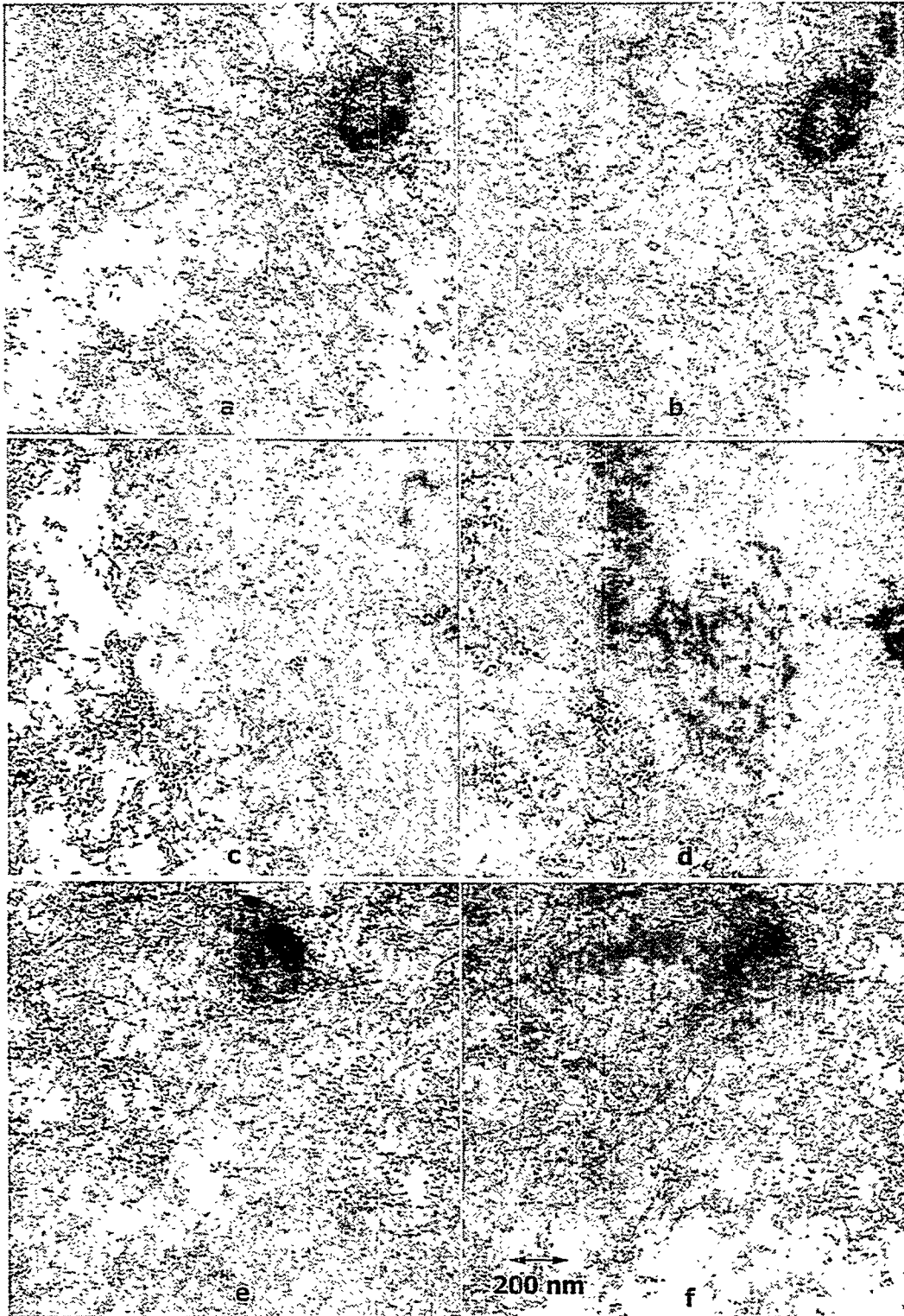


Figure 7. Stereo pair images of the dislocation structure found in specimen AR17 showing  $g = \bar{1}01, 002$  and  $01\bar{1}$  in a) and b), c) and d), and e) and f), respectively with  $g$  vertical in all cases.

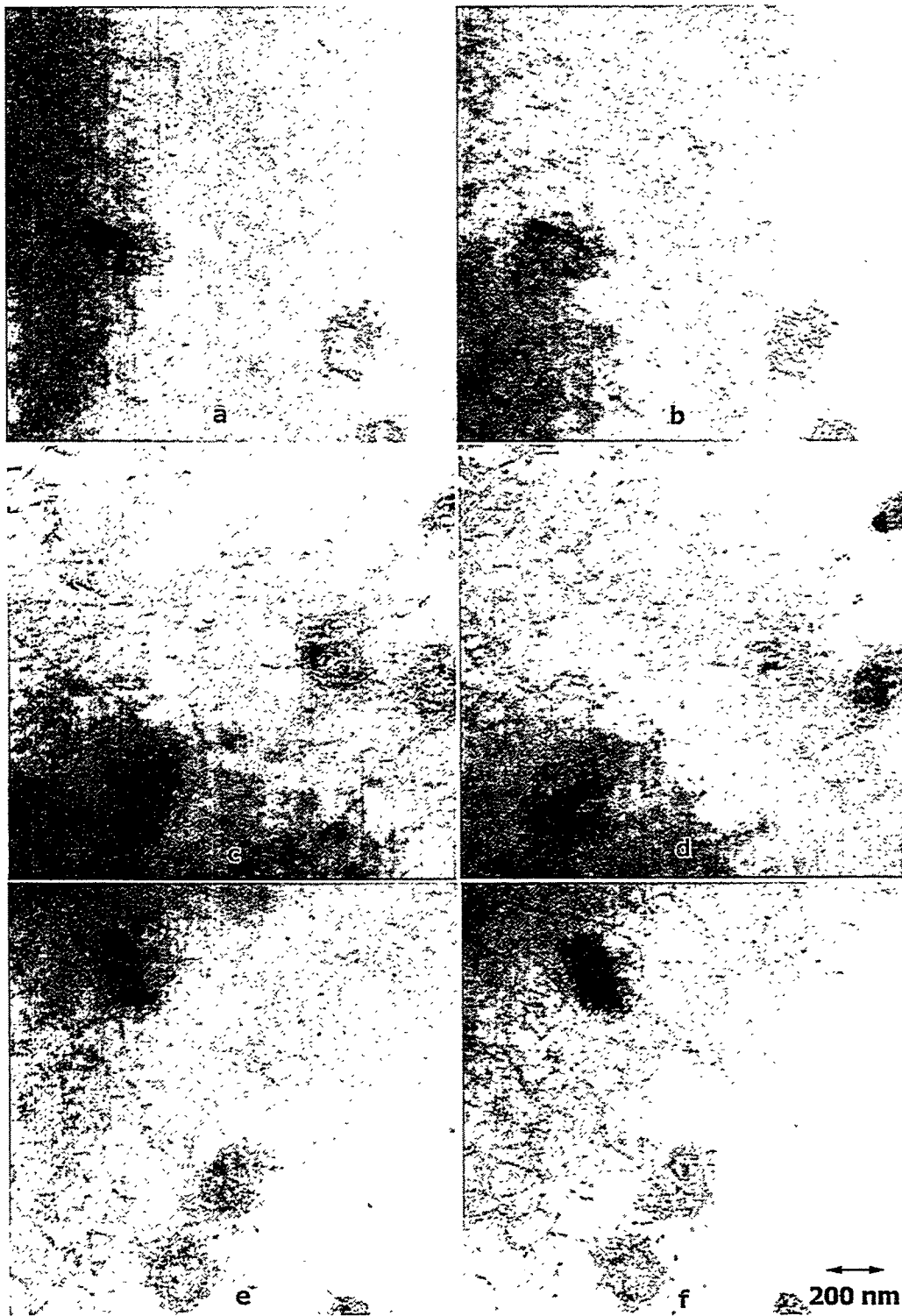


Figure 8. Stereo pair images of the dislocation structures found in specimen AR19 showing  $g=\bar{1}01, 002$  and  $01\bar{1}$  in a) and b), c) and d), and e) and f), respectively with  $g$  vertical in all cases.

Finally, Figure 9 is provided, showing examples of the dislocation structure found in specimen AR15, tested at 700°C. In each case, contrast is due to  $\langle 011 \rangle$  but the region was not considered sufficiently uniform to provide a stereo sequence. Figure 9 demonstrates that dislocation evolution during thermal creep at 700°C is similar to that found at 800°C

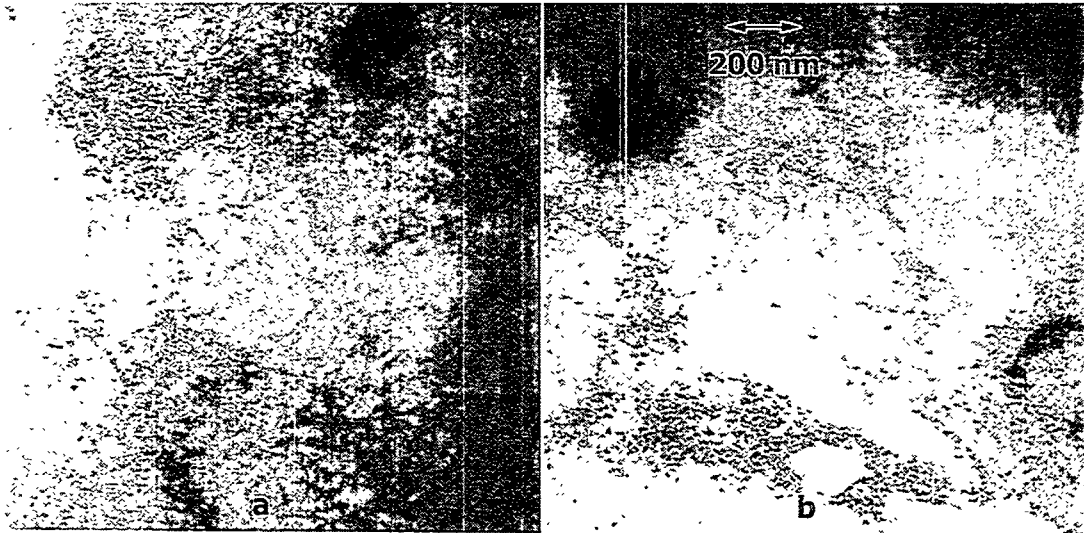


Figure 9. Examples of dislocation structures found in specimen AR15.

### Discussion

Creep measurements using pressurized tube techniques are inevitably limited by the quality of the tubing used. Figures 3 and 4 reveal a number of small longitudinal defects and figure 5 indicates that where large strains have occurred, strain can be very non-uniform, showing that surface defects probably played a role in strain localization. SEM investigations also revealed larger inner surface defects such as radial scratches or gouges, but those examples are not included in this report because they apparently did not play a role in failure. It is therefore possible that failure to observe steady state creep response during biaxial thermal creep testing of V-4Cr-4Ti could be a consequence of internal surface defects. Also, rupture times can be expected to be underestimates for bulk material. Nonetheless, the quality of the tubing used is demonstrably adequate to provide good estimates for bulk thermal creep properties.

Figures 5 b) and e) can be interpreted to indicate that oxidation occurred on the outer surface of specimen AR17 during testing. Unfortunately, the dark banding on one side of the tube is believed due to staining, a metallographic artifact. This can be corroborated based on oxygen content measurements. An unpressurized control specimen in the 800°C furnace beside the pressurized tubes contained 59.8 wppm N and 733 wppm O. Therefore, the increase in the oxygen content was on the order of 30% over the levels after fabrication of 560 wppm.<sup>2</sup> Also, calculations indicated that oxygen penetration for the relevant time and temperature should be on the order of 2000  $\mu\text{m}$ , approximately ten times the thickness of the stain.

The microstructures found following thermal creep indicate that strain is controlled by dislocation climb. This is confirmed by the elongated grain structure shown in figures 5 a), b) and c) and in

agreement with the high stress exponent found for other tests.<sup>1</sup> However, it is also apparent that  $\text{TiO}_2$  plays a role in controlling creep rates by acting as obstacles to dislocation climb. And the consequences of the small features expected to be  $\text{Ti(O,C,N)}$  precipitation are not yet understood. The lack of a well-defined dislocation cell structure, and therefore, a well-defined cell size, is possibly a consequence of the lack of steady state creep response.

A concern with the microstructural observations is that specimen preparation procedures may have affected the observed dislocation structures. TEM specimen preparation using ultrasonic drilling has not been used in the past, but was warranted because of the variation in tube diameter found following creep testing. As control specimens were not prepared, it cannot be shown conclusively that ultrasonic preparation has not influenced the results. Also, although most dislocation images appear to be typical of climbing dislocations, the stereo pair of figures 7e) and f) can be interpreted to contain a large number of slip dislocations oriented for optimum slip.

## CONCLUSIONS

Failed V-4Cr-4Ti biaxial thermal creep specimens have been examined using OM, SEM and TEM in order to assess creep and failure mechanisms. It was found that deformation is probably due to dislocation climb, influenced by  $\text{TiO}_2$  precipitation, and that lack of steady state creep response could be due to minor tube defects.

## FUTURE WORK

This work will be continued within the confines of funding and specimen availability.

## REFERENCES

1. R. J. Kurtz and M. L. Hamilton, DOE/ER-0313/25 (1999) 7.
2. H. Tsai, M. C. Billone, R. V. Strain, and D. L. Smith, DOE/ER-0313/23 (1998) 149.
3. D.S. Gelles, A. Kimura and R. J. Puigh, DOE/ER-0313/12 (1992) 123.
4. D. S. Gelles and H. Li, DOE/ER-0313/19 (1995) 22.